ARTICLE

Giant Thermoelectric Effect from Transmission Supernodes

Justin P. Bergfield,[†,*] Michelle A. Solis,[‡] and Charles A. Stafford[‡]

[†]College of Optical Sciences, University of Arizona, 1630 East University Boulevard, Arizona 85721 and [‡]Department of Physics, University of Arizona, 1118 East Fourth Street, Tucson, Arizona 85721

ABSTRACT We predict an enormous order-dependent quantum enhancement of thermoelectric effects in the vicinity of higher-order interferences in the transmission spectrum of a nanoscale junction. Single-molecule junctions based on 3,3′-biphenyl and polyphenyl ether (PPE) are investigated in detail. The nonequilibrium thermodynamic efficiency and power output of a thermoelectric heat engine based on a 1,3-benzene junction are calculated using many-body theory and compared to the predictions of the figure-of-merit ZT.

KEYWORDS: many-body theory · nonequilibrium transport · molecular electronics · ZT · thermoelectrics · electron transport · nanoscale device · thermoelectric device

Thermoelectric (TE) devices are highly desirable since they can directly convert between thermal and electrical energy. Electrical power can be supplied to such a device to either heat or cool adjoining reservoirs (Peltier effect), or, alternatively, the flow of heat (*e.g.*, from a factory or car exhaust) can be converted into usable electrical power (Seebeck effect). Often, the efficiency of a TE device is characterized by the dimensionless figure-of-merit $ZT = S^2GT/\kappa$, constructed with the rationale that an efficient TE device should simultaneously maximize the electrical conductance G so that current can flow without much Joule heating, minimize the thermal conductance κ in order to maintain a temperature gradient across the device, and maximize the Seebeck coefficient S to ensure that the coupling between the electronic and thermal currents is as large as possible.[1,2] Generally, however, ZT is difficult to maximize because these properties are *highly correlated* with one another,[3−5] a fact that becomes more pronounced at the nanoscale where the number of degrees of freedom available is small.

If a TE material were found exhibiting $ZT \geq 4$ it would constitute a commercially viable solution for many heating and cooling problems at both the macro- and nanoscales, with no operational carbon footprint.[2] Currently, the best TE materials available in the laboratory exhibit $ZT \approx 3$, whereas for commercially available TE devices $ZT \approx 1$, owing to various packaging and fabrication challenges.[1,6]

In a previous article, enhanced thermoelectric effects were found in the vicinity of a transmission node of a quantum tunneling device.[7] Generically, the transmission probability vanishes quadratically as a function of energy at such a transmission node. Here we present results for a class of two-terminal single-molecule junctions (SMJs) with higher-order "supernodes" in their transmission spectra. In the vicinity of a $2n^{th}$ order supernode:

$$T(E) \propto (E - \mu_{node})^{2n} \qquad (1)$$

where μ_{node} is the energy of the node. We find that junctions possessing such supernodes exhibit a scalable order-dependent quantum-enhanced thermoelectric response.

As an example, ZT of a supernode-possessing polyphenyl ether (PPE)-based SMJ is shown as a function of repeated phenyl unit number n in Figure 1. As illustrated in the figure, the maximum value of ZT^{el}, the figure of merit for purely electronic transport, scales superlinearly in n whereby $\max\{ZT^{el}\} = 4.1$ in a junction composed of just four phenyl groups ($n = 4$). Although we focus on molecular junctions in this article, it should be stressed that our results are applicable to any device with transmission nodes arising from coherent electronic transport. In addition to higher-order destructive interferences, we find that higher-order *constructive* interferences also strongly enhance thermoelectric effects.

As an engineering rule-of-thumb, ZT has been widely used to characterize the bulk

*Address correspondence to justinb@email.arizona.edu.

Received for review March 10, 2010 and accepted August 2, 2010.

Published online August 24, 2010. 10.1021/nn100490g

thermoelectric response of materials.[1,2,5] At the nanoscale, however, it is unclear the extent to which ZT is applicable, since bulk scaling relations for transport may break down due to quantum effects.[8] Moreover, ZT is a linear response metric, and cannot *a priori* predict nonequilibrium thermoelectric response.

We investigate the efficacy of ZT as a predictor of *nonequilibrium device performance* at the nanoscale by calculating the thermodynamic efficiency and power of an interacting quantum system using both nonequilibrium many-body[9] and Hückel theories. We discover that in both theories, variations of ZT and thermodynamic efficiency are in good qualitative agreement. However, significant discrepancies between thermoelectric effects calculated within many-body and Hückel theory are found in the resonant tunneling regime, indicating the essential role of electron−electron interactions in nanoscale thermoelectricity. For a thermoelectric quantum tunneling device, we find that the power output can be changed significantly by varying an external parameter, such as a gate voltage, and that this variation is *not correlated* with the variation of ZT.

Thermoelectric Theory. Neglecting inelastic processes, which are strongly suppressed at room temperature in SMJs, the current flowing into lead 1 of a two-terminal junction may be written as follows:[7]

$$I_1^{(\nu)} = \frac{1}{h}\int_{-\infty}^{\infty} dE(E-\mu_1)^{\nu} T(E)[f_2(E) - f_1(E)] \qquad (2)$$

where $\nu = 0$ ($\nu = 1$) for the number (heat) current, $f_\alpha(E)$ is the Fermi function for lead α with chemical potential μ_α and inverse temperature β_α, and $T(E)$ is the transmission probability for an electron of energy E to tunnel across the junction. This transmission function may be expressed in terms of the junction's Green's functions as[8]

$$T(E) = \mathrm{Tr}\{\Gamma^1(E)\, G(E)\, \Gamma^2(E)\, G^\dagger(E)\} \qquad (3)$$

where $\Gamma^\alpha(E)$ is the tunneling-width matrix for lead α and $G(E)$ is the retarded Green's function of the SMJ.

In organic molecules, such as those considered here, electron−phonon coupling is weak, allowing ZT to be expressed as follows:

$$ZT = ZT^{el}\left(\frac{1}{1+\kappa^{ph}/\kappa^{el}}\right) \qquad (4)$$

where[10]

$$ZT^{el} = \left(\frac{\mathscr{L}^{(0)}\mathscr{L}^{(2)}}{[\mathscr{L}^{(1)}]^2} - 1\right)^{-1} \qquad (5)$$

and

$$\mathscr{L}^{(\nu)}(\mu) = \frac{1}{h}\int dE(E-\mu)^{\nu} T(E)\left(-\frac{\partial f_0}{\partial E}\right) \qquad (6)$$

Here f_0 is the equilibrium Fermi function and $\kappa^{ph} = \kappa_0 T^{ph}$ is the phonon's thermal conductance, where $\kappa_0 = (\pi^2/3)(k_B^2 T/h)$ is the thermal conductance quantum[11] and T^{ph} is the phonon transmission probability. The electronic thermal conductance is given by

$$\kappa^{el} = \frac{1}{T}\left(\mathscr{L}^{(2)} - \frac{[\mathscr{L}^{(1)}]^2}{\mathscr{L}^{(0)}}\right) \qquad (7)$$

where T is the temperature.

The phonon thermal conductance of the junction is typically limited by the lead-molecule interface.[12] Since the Debye frequency in the metal lead is typically smaller than the lowest vibrational mode of a small organic molecule, the spectral overlap of phonon modes between the two is small, implying $T^{ph} \ll 1$, so that $\kappa^{ph} \ll \kappa_0$. Nonetheless, it is claimed that κ^{ph} can reach values as large as 10^{-10} W/K for some SMJs,[12,13] so the correction to ZT due to phonon heat transport (*cf.* eq 4) must be taken into account for quantitative estimates of device performance.[14] Let us first consider purely electronic transport; the effect of phonons will be discussed at the end of this article.

Thermodynamically, a system's response is characterized by the efficiency η with which heat can be converted into usable power P and the amount of power that can be generated. Applying the first law of thermodynamics to the device shown in Figure 2 gives

$$P = -I_1^{(1)} - I_2^{(1)} = I_1^{(0)}(\mu_1 - \mu_2) \qquad (8)$$

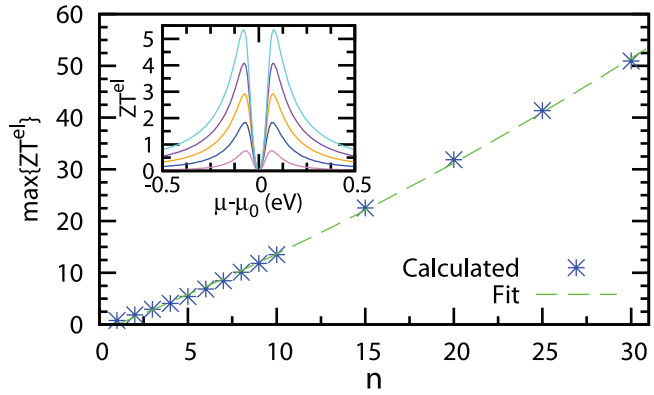

Figure 1. Near a $2n^{th}$ order *supernode* in a device's transmission spectrum, we find an order-dependent enhancement of the electronic thermoelectric response which is limited only by the electronic coherence length. Calculations were performed for a polyphenyl ether (PPE) SMJ with n repeated phenyl groups at room temperature ($T = 300$ K) with $\Gamma = 0.5$ eV. Notice that the enhancement is superlinear in n. Inset: ZT as a function μ for $n = 1-5$.

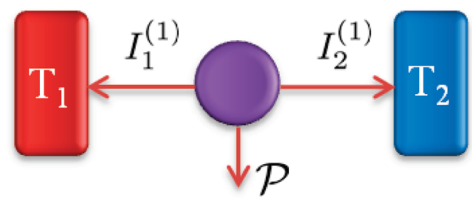

Figure 2. Schematic diagram of a thermoelectric device, where $I_\alpha^{(1)}$ is the heat current flowing into lead α, T_α is the temperature, and P is the power output.

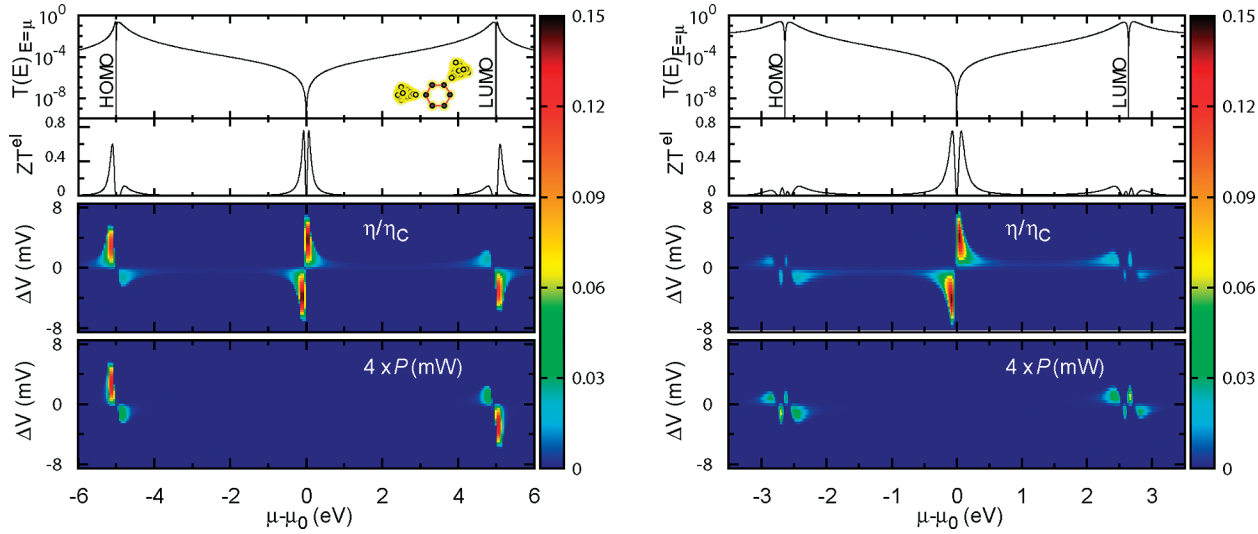

(a) many-body theory (b) Hückel theory

Figure 3. The transmission probability $T(E)$, figure-of-merit ZT^{el}, Carnot-normalized efficiency η/η_C, and electrical power output P of a two-terminal 1,3-benzene SMJ, with lead temperatures $T_1 = 300$ K and $T_2 = 250$ K, calculated using (a) many-body and (b) Hückel theory, highlighting the discrepancies near resonances and the similarities near the node in the two theories. As a function of μ, η and ZT^{el} are in excellent qualitative agreement while P is only peaked near resonance, suggesting that ZT is incomplete as a device performance metric. (a) Many-body calculations give $P_{peak} = 33$ μW and $\eta_{peak}/\eta_C = 11.5\%$ near resonance. (b) Hückel calculations give $P_{peak} = 21$ μW and $\eta_{peak}/\eta_C = 2.7\%$ near resonance. The midgap region is discussed in Figure 4. Note that the peak $ZT^{el} = 0.75$ is on par with currently available commercial thermoelectrics.[1,5] Calculations were performed using the model and parametrization of benzene discussed in detail in ref 9 with $\Gamma = 0.63$ eV.

where we mention that the power is equivalently phrased in terms of heat or electrical currents. The efficiency η is defined as the ratio of power output to input heat current:

$$\eta = \frac{P}{|I_1^{(1)}|} = -\frac{I_1^{(1)} + I_2^{(1)}}{|I_1^{(1)}|} \qquad (9)$$

where we have assumed that $T_1 > T_2$. With these expressions for the power and efficiency, we can completely quantify the performance of a quantum device, both near and far from equilibrium.

RESULTS AND DISCUSSION

1,3-Benzenedithiol-Au Junction. As a first example, we calculate the nonlinear thermoelectric response of a meta-connected Au−benzene−Au SMJ using many-body[9] and Hückel theory, shown in Figure 3a and Figure 3b, respectively. Although the transmission spectrum of this junction does not possess a supernode, it does possess a quadratic node within π-electron theory,[7,15] and will allow us to ascertain the importance of interactions on the thermoelectric response of a SMJ.

Additional transport channels (*e.g.*, from σ-orbitals) or incoherent scattering may lift the transmission node. The effect on the thermoelectric response is small provided these processes are weak, as discussed in ref 7. The effect of σ-orbitals in SMJs whose π-orbitals exhibit an ordinary node was investigated in ref 16. Because the σ transmission is exponentially suppressed[16,17] as the length of the molecule increases, the effect of the σ-orbitals should be quantitatively insignificant in the biphenyl and larger molecules considered below.

In the top panels of Figure 3 is a section of the transmission spectrum, showing the HOMO and LUMO resonances and the quadratic node directly in between at $\mu = \mu_0$. Associated with this node is an enhancement in many linear-response metrics[7] including ZT, which is shown in the second panel from the top. The bottom two portions of each figure show the calculated efficiency η and power P when a junction with $T_1 = 300$ K and $T_2 = 250$ K is further pushed out of equilibrium via the application of a bias voltage ΔV. In all simulations presented here, the lead-molecule coupling is taken to be symmetric such that $\Gamma^{\alpha}_{nm} = \Gamma\delta_{n\alpha}\delta_{m\alpha}$, where n, m, and a are π-orbital labels and a is coupled to lead α. The efficiency is normalized with respect to the maximum allowed by the second law of thermodynamics, the Carnot efficiency $\eta_C = \Delta T/T_1$, where $\Delta T = T_1 - T_2$.

The nonequilibrium thermodynamic response of a 1,3-benzene SMJ calculated using many-body theory is shown in Figure 3a. The ZT and η spectra, shown in two middle panels of the same figure, exhibit peaks in the vicinity of both transmission nodes and resonances, whereas the power P, shown in the bottom panel, is only peaked near transmission resonances. Around either the HOMO or LUMO resonance, the peak power $P_{peak} = 33$ μW and peak efficiency $\eta_{peak}/\eta_C = 11.5\%$ are only realized when the junction operates out of equilibrium at a bias voltage $\Delta V = 3$ mV. With a chemical potential near the

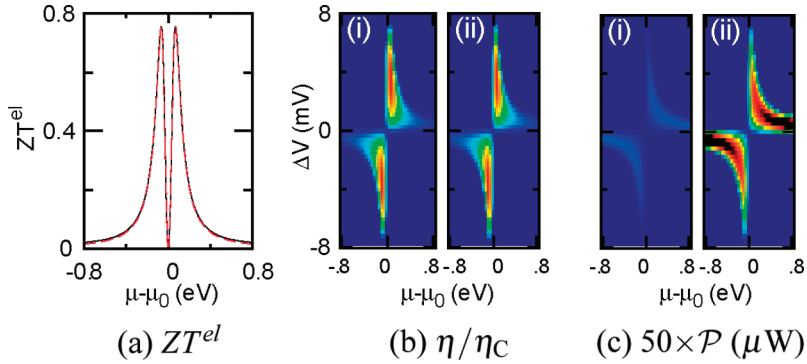

Figure 4. Calculations of ZT, η, and *P* in the vicinity of the transmission node at $\mu = \mu_0$ of a meta-benzene SMJ using many-body (red line and panel i) and Hückel (black line and panel ii) theories. (a and b): ZT and η are found to be identical and independent of theory. (c) *P* is strongly affected by interactions where, at peak efficiency ($\eta_{peak}/\eta_C = 14.91\%$), many-body and Hückel calculations give $P_{max} = .088$ nW and $P_{max} = 1.87$ nW, respectively. The simulation parameters and colorscale are the same as in Figure 3.

midgap node and $\Delta V = 3.6$ mV $\eta_{peak}/\eta_C = 14.9\%$, larger than near resonance but with a much lower peak power $P_{peak} = .088$ nW.

In the vicinity of a resonance, there are both quantitative and qualitative differences in the linear and nonlinear thermodynamic response predicted by the two theories. By neglecting interactions, the Hückel theory fails to accurately predict both the degeneracy and position of electronic resonances. It also incorrectly determines the peak values of ZT, η, and *P* in the vicinity of a resonance. As can be seen near either (HOMO or LUMO) resonance in Figure 3, the Hückel theory predicts a Carnot-normalized peak efficiency of 2.7% which is nearly five times less than the 11.5% predicted by the many-body theory. The peak power near a resonance also varies considerably between the two theories, where the Hückel calculations give $P_{peak} = 21$ μW while many-body theory predicts $P_{peak} = 33$ μW. These results indicate that interactions are required to accurately predict the thermoelectric response of devices operating in the resonant-tunneling regime. It is interesting to note, however, that in both models the linear-response metric ZT qualitatively captures the features of the nonlinear metric η.

In this article, we are interested in thermoelectric enhancement near nodes far away from any resonances. Although interactions are *required* in order to ensure the invariance of transport quantities under a global voltage shift (*i.e.*, gauge-invariance), near the particle-hole symmetric point the effect of interactions on the thermoelectric response should be small. In panels a and b of Figure 4, a comparison of ZT and η using both many-body and Hückel theories is shown near μ_0 for a 1,3-benzene SMJ. Near this point, ZT and η are independent of theory employed. In contrast, the power, shown in panel c of the same figure, exhibits an order of magnitude difference between the two theories. This observation can be understood by noticing that the calculated HOMO−LUMO gap is ~10 eV using many-body theory (panel c-i), whereas it is only ~5.5 eV when interactions are neglected in the Hückel theory (panel c-ii). Since the power is peaked near transmission resonances, whose widths are fixed by the lead-molecule coupling Γ, the larger gap found using many-body theory gives a correspondingly lower predicted power.

While the Hückel theory does not accurately characterize the thermoelectric response of a junction in the resonant-tunneling regime, it is sufficient for predicting η and ZT in the vicinity of the transmission node. Since we are interested in these quantities for midgap supernodes, we shall use Hückel theory to simulate the larger molecules presented below.

The transmission node in a meta-benzene junction can be understood in terms of destructive interference of electron waves traversing the ring at the Fermi energy.[15] According to Luttinger's theorem,[18] the Fermi volume is unaffected by the inclusion of electron−electron interactions. Consequently, in an aromatic ring such as benzene the Fermi wavevector $k_F = \pi/2d$, where *d* is the intersite distance, is conserved and is therefore sufficient to characterize quantum in-

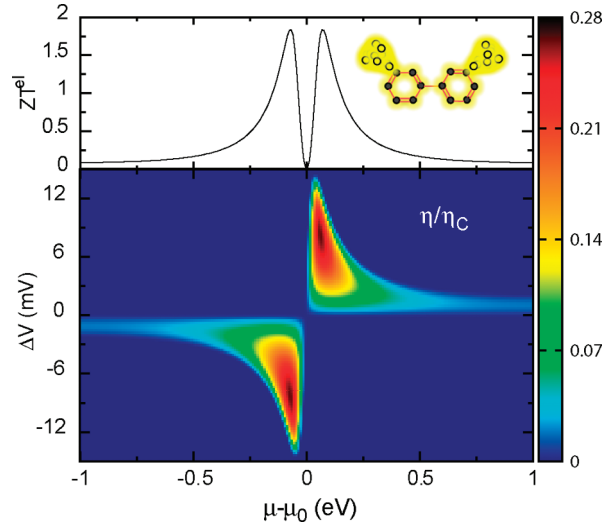

Figure 5. A closeup of ZT and η near the quartic supernode of a 3,3′-biphenyl SMJ showing $ZT_{peak} = 1.84$ and $\eta_{peak}/\eta_C = 26.86\%$ at a predicted power of 0.75 pW. The junction geometry is shown schematically in the inset of the upper panel. Simulations were performed using Hückel theory with $T_1 = 300$ K, $T_2 = 250$ K and $\Gamma = 0.5$ eV.

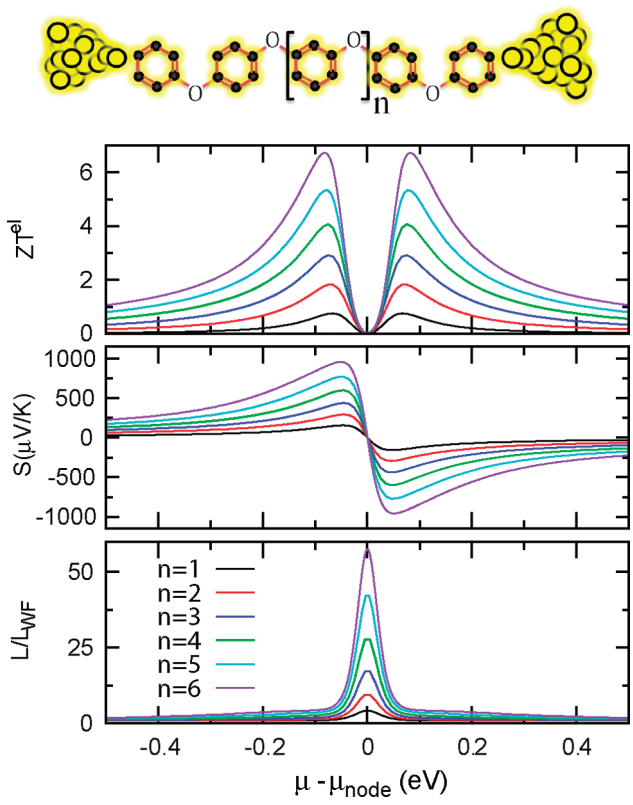

Figure 6. Supernode enhancement of ZT, thermopower *S*, and Lorenz number *L* for polyphenyl ether (PPE) SMJs with *n* repeated phenyl groups, shown schematically above the top panel. As a function of *n*, ZT_{peak} scales superlinearly exhibiting a peak value of 6.86 for $n = 6$. The thermopower and Lorenz number are also enhanced with $S_{peak} = 957\ \mu V/K$ and $L_{peak} = 55.33L_{WF}$ at the same value of *n*. Simulations were performed using Hückel theory at room temperature ($T = 300$ K) with $\Gamma = 0.5$ eV. Interphenyl electronic hopping was set an order of magnitude below the intraphenyl value of 2.64 eV.

terference both with and without interactions near μ_0 since $\Delta\phi = k_F\Delta l$, where $\Delta\phi$ is the relative phase between transport paths with length difference Δl.

The Effect of Higher-Order Interferences. This is an important result, since the energy of resonant levels will generally depend strongly on whether or not interactions are included. Since k_F is protected, however, the transmission node across a single phenyl group is not so much a coincidence of energy levels as a *wave phenomenon*, meaning that interference in molecules composed of multiple aromatic rings in series can be understood in terms of the interference within each subunit rather than the energy spectrum of the entire molecule. We find that such polycyclic molecules can exhibit higher-order *supernodes* and that associated with a supernode is an order-dependent quantum enhancement of the junction's thermoelectric response.

The 3,3′-biphenyl junction, drawn schematically in the top panel of Figure 5, can be viewed as two meta-connected benzene rings in series. This junction geometry is similar to that studied by Mayor *et al.*[19] In agreement with the prediction that a biphenyl junction should possess a quartic supernode, the linear and nonlinear response shown in Figure 5 exhibits peak values of efficiency ($\eta/\eta_C = 26.86\%$) and ZT^{el} (1.84) that are over twice those of benzene. With $ZT \approx 2$, the biphenyl junction exhibits sufficient thermoelectric performance to be attractive for many commerical solid-state heating and cooling applications.[1,2,5] As we shall see, this is only the first in an entire class of supernode-possessing molecules which exhibit even larger values of η and ZT.

In larger molecules composed of *n* meta-connected phenyl groups in series, we expect that the transmission nodes should combine and give rise to a $2n^{th}$ order supernode. Polyphenyl ether (PPE), shown schematically at the top of Figure 6, consists of *n* phenyl rings connected in series with ether linkages. On the basis of our previous discussion, we predict that a PPE-based junction should exhibit a $2n^{th}$ order supernode. The figure-of-merit ZT, thermopower *S*, and Lorenz number $L = \kappa/GT$ for PPE junctions are shown in the top, middle, and bottom panels of Figure 6, respectively, where the Lorenz number is normalized with respect to the Wiedemann−Franz (WF) value $L_{WF} = (\pi^2/3)(k_B/e)^2$.

The bottom panel of Figure 6 shows an increasing peak Lorenz number L_{peak} with increasing *n*. In linear-response, *L* and *S* can be expressed in terms of eq 6 as

$$L|_{el} = \frac{1}{(eT)^2}\left(\frac{\mathscr{L}^{(2)}}{\mathscr{L}^{(0)}} - \left[\frac{\mathscr{L}^{(1)}}{\mathscr{L}^{(0)}}\right]^2\right) \qquad (10)$$

and

$$S = -\frac{1}{eT}\frac{\mathscr{L}^{(1)}}{\mathscr{L}^{(0)}}$$

where *e* is the magnitude of the electron's charge and *T* is the temperature. Using eq 10 and eq 6 with the transmission function of eq 1 we find that

$$\left.\frac{L_{max}}{L_{WF}}\right|_{el} = \left(\frac{3}{\pi^2}\right)\frac{[\partial_b^{2n+2} b\pi \csc(b\pi)]|_{b=0}}{[\partial_b^{2n} b\pi \csc(b\pi)]|_{b=0}} \qquad (11)$$

Setting $n = 6$ in eq 11 gives $L_{max} = 55.33L_{WF}$, corresponding exactly to the result of the full simulation shown in the bottom panel of Figure 6. Similar agreement is found for the other values of *n*, confirming the presence of $2n^{th}$ order supernodes in these junctions.

The above discussion considered purely electronic transport. According to eq 4, phonon heat transport may reduce ZT significantly,[14] although it should be emphasized that the thermopower of the junction is unaffected provided the electron−phonon coupling is negligible. Figure 7 shows the effect of phonon heat transport on ZT of a 3,3′-biphenyl junction for several values of the phonon transmission probability T^{ph}. In the vicinity of the quartic transmission node, ZT is significantly reduced even for small values of T^{ph}. However, the large peaks of ZT found near the transmission resonances are largely insensitive to phonon heat transport due to the smaller ratio of κ^{ph}/κ^{el}. Practical supernode-based devices will thus require careful engi-

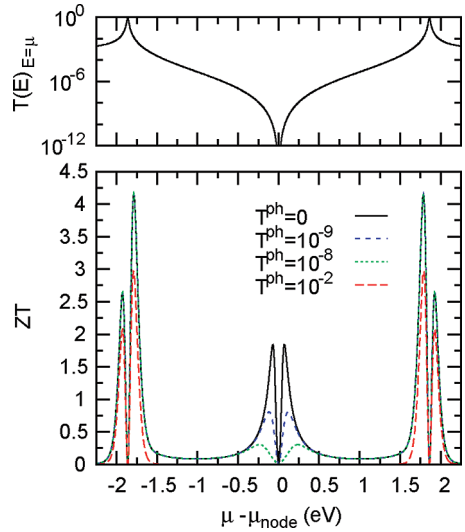

Figure 7. The transmission probability $T(E)$ and ZT for a 3,3′-biphenyl SMJ with several different phonon transmission values. Although phonon transport strongly reduces ZT near the supernode, the enhancement of ZT near the transmission peaks is fairly insensitive to moderate values of T^{ph}. Recall that $\kappa^{ph} = \kappa_0 T^{ph}$.

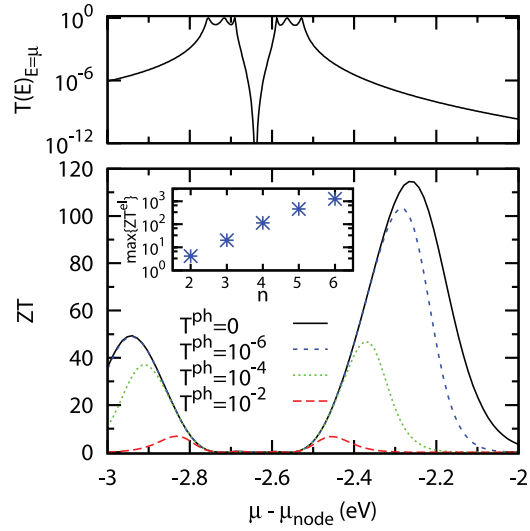

Figure 8. The transmission and ZT in the vicinity of a transmission peak for a tetraphenyl ether ($n = 4$) molecule showing that ZT^{el} is enhanced in the vicinity of a higher-order peak. Inset: the maximal ZT^{el} value found near a $2n^{th}$ order transmission peak is shown on a log scale.

neering of phonon transport. For example, the inclusion of a vacuum tunneling gap in series with the junction would effectively block phonon transport.

Higher-order quantum interference effects can arise from both destructive and constructive interference. As evidenced by Figure 7, thermoelectric devices based on constructive interference are far less sensitive to phonon effects. Figure 8 shows the transmission spectrum and ZT^{el} near the HOMO resonance of a tetraphenyl ether SMJ. The transmission resonance exhibits fine structure due to electronic standing waves along the molecular chain.[20] The interplay of the many closely spaced resonances gives rise to a dramatic enhancement of the thermopower in a regime of large electrical conductance, and hence a very large $ZT^{el} \approx 10^2$. The inset of Figure 8 shows the exponential scaling of the peak ZT^{el} near the HOMO resonance of a polyphenyl ether SMJ as a function of the phenyl group number n. The predicted giant enhancement of ZT^{el} occurs over a broad energy range, in contrast to that expected from a narrow transmission resonance.[10]

CONCLUSIONS

We find that higher-order quantum interferences in the transmission spectrum of a nanoscale junction give rise to an order-dependent quantum-enhancement of the linear and nonlinear thermoelectric response. The full nonequilibrium spectrum of thermodynamic efficiency qualitatively resembles the figure-of-merit ZT spectrum, suggesting that ZT encapsulates the salient physics related to efficiency even at the nanoscale. Efficiency, however, is only part of a device's performance. Another important quantity is the usable power produced by a device, whose variations are poorly characterized by ZT at the nanoscale.

Thermoelectric devices based on individual SMJs are ideally suited for local cooling in integrated nanoscale circuit architectures. Supernode-based devices have a low transmission probability and thus a large electrical impedance capable of withstanding voltage surges. In contrast, devices based on higher-order constructive interference are more robust with respect to phonon heat transport. High-power macroscopic devices could be constructed by growing layers of densely packed molecules. For example, a self-assembled monolayer with a surface density[21] of 4×10^{15} molecules/cm^2 would give 352 kW/cm^2 at peak efficiency for a meta-benzene film. The efficiency of PPE-based devices increases with ring number and is limited only by the electronic coherence length and phonon heat transport, suggesting that highly efficient molecular-based thermoelectric devices may soon be realized.

METHODS

The Green's function of a SMJ has the form[9]

$$G(E) = [G_{mol}^{-1}(E) - \Sigma_T(E) - \Delta\Sigma_C(E)]^{-1} \qquad (12)$$

where G_{mol} is the molecular Green's function, Σ_T is the tunneling self-energy matrix, whose imaginary part is given by $\mathrm{Im}\Sigma_T = -\Sigma_\alpha \Gamma^\alpha/2$, and $\Delta\Sigma_C$ is the correction to the Coulomb self-energy due to the broadening of the molecular resonances in the junction. At room temperature and for small bias voltages, $\Delta\Sigma_C \approx 0$ in the cotunneling regime[9] (*i.e.*, for nonresonant transport). Furthermore, the inelastic transmission probability is negligible compared to eq 3 in that limit.

The molecular Green's function G_{mol} is found by exactly diagonalizing the molecular Hamiltonian, projected onto a basis of relevant atomic orbitals:[9]

$$G_{\mathrm{mol}}(E) = \sum_{\nu,\nu'} \frac{[\mathscr{P}(\nu) + \mathscr{P}(\nu')]C^{\nu\nu'}}{E - E_{\nu'} + E_{\nu} + i\,0^{+}} \tag{13}$$

where E_ν is the eigenvalue associated with eigenstate ν of the molecular Hamiltonian, $\mathscr{P}(\nu)$ is the probability that the state ν is occupied, and $C^{\nu\nu'}$ is a matrix with elements

$$[C^{\nu\nu'}]_{n\sigma,m\sigma'} = \langle\nu|d_{n\sigma}|\nu'\rangle\langle\nu'|d^{\dagger}_{m\sigma'}|\nu\rangle \tag{14}$$

Here $d_{n\sigma}$ annihilates an electron of spin σ on the nth atomic orbital of the molecule. For linear response, $\mathscr{P}(\nu)$ is given by the grand canonical ensemble.

A semiempirical π-electron Hamiltonian that accurately describes Coulomb interactions and π-conjugation was used to model the electronic degrees of freedom most relevant for transport:

$$H_{\mathrm{mol}} = \sum_{n,\sigma} \varepsilon_n d^{\dagger}_{n\sigma} d_{n\sigma} - \sum_{n,m,\sigma} (t_{nm} d^{\dagger}_{n\sigma} d_{m\sigma} + \mathrm{H.c.}) + \sum_{n,m} \frac{U_{nm}}{2} Q_n Q_m \tag{15}$$

where ε_n is the π-orbital energy, t_{nm} is the hopping matrix element between orbitals n and m, U_{nm} is the effective interaction energy between orbitals n and m, and the effective charge operator for orbital n is[9,15,22]

$$Q_n = \sum_{\sigma} d^{\dagger}_{n\sigma} d_{n\sigma} - \sum_{\alpha} C_{n\alpha} \mathscr{V}_{\alpha}/e - 1 \tag{16}$$

where $C_{n\alpha}$ is the capacitive coupling between orbital n and lead α, e is the electron charge, and $\mathscr{V}_\alpha$ is the voltage on lead α.

The effective interaction energies for π -conjugated systems can be written[23]

$$U_{nm} = \delta_{nm} U_0 + (1 - \delta_{nm}) \frac{U_0}{\varepsilon\sqrt{1 + \alpha(R_{nm})^2}} \tag{17}$$

where U_0 is the on-site Coulomb repulsion, $\alpha = (U_0/14.397\ \mathrm{eV})^2$, and R_{nm} is the distance between orbitals n and m in angstroms. The phenomenological dielectric constant ε accounts for screening due to both the σ-electrons and any environmental considerations, such as nonevaporated solvent.[23]

The Hamiltonian parameters used for each phenyl ring were[23] $U_0 = 8.9$ eV, $\varepsilon = 1.28$, $t_{nm} = 2.64$ eV for n and m nearest neighbors, and $t_{nm} = 0$ otherwise. We only consider symmetric junctions in this article (symmetric capacitive couplings and $\Gamma = \Gamma_1 = \Gamma_2$).

REFERENCES AND NOTES

1. Bell, L. E. Cooling, Heating, Generating Power, and Recovering Waste Heat with Thermoelectric Systems. *Science* **2008**, *321*, 1457–1461.
2. DiSalvo, F. J. Thermoelectric Cooling and Power Generation. *Science* **1999**, *285*, 703–706.
3. Hochbaum, A. I.; Chen, R.; Delgado, R. D.; Liang, W.; Garnett, E. C.; Najarian, M.; Majumdar, A.; Yang, P. Enhanced Thermoelectric Performance of Rough Silicon Nanowires. *Nature* **2008**, *451*, 163–167.
4. Majumdar, A. Thermoelectricity in Semiconductor Nanostructures. *Science* **2004**, *303*, 777–778.
5. Snyder, G. J.; Toberer, E. S. Complex Thermoelectric Materials. *Nat. Mater.* **2008**, *7*, 105–114.
6. Harman, T. C.; Taylor, P. J.; Walsh, M. P.; LaForge, B. E. Quantum Dot Superlattice Thermoelectric Materials and Devices. *Science* **2002**, *297*, 2229–2232.
7. Bergfield, J. P.; Stafford, C. A. Thermoelectric Signatures of Coherent Transport in Single-Molecule Heterojunctions. *Nano Lett.* **2009**, *9*, 3072–3076.
8. Datta, S. In *Electronic Transport in Mesoscopic Systems*; Cambridge University Press: Cambridge, UK, 1995; pp 117−174.
9. Bergfield, J. P.; Stafford, C. A. Many-Body Theory of Electronic Transport in Single-Molecule Heterojunctions. *Phys. Rev. B* **2009**, *79*, 245125.
10. Finch, C. M.; García-Suárez, V. M.; Lambert, C. J. Giant Thermopower and Figure of Merit in Single-Molecule Devices. *Phys. Rev. B* **2009**, *79*, 033405.
11. Rego, L. G. C.; Kirczenow, G. Fractional Exclusion Statistics and the Universal Quantum of Thermal Conductance: A Unifying Approach. *Phys. Rev. B* **1999**, *59*, 13080–13086.
12. Wang, Z.; Carter, J. A.; Lagutchev, A.; Koh, Y. K.; Seong, N.; Cahill, D. G.; Dlott, D. D. Ultrafast Flash Thermal Conductance of Molecular Chains. *Science* **2007**, *317*, 787–790.
13. Segal, D.; Nitzan, A.; Hänggi, P. Thermal Conductance through Molecular Wires. *J. Chem. Phys.* **2003**, *119*, 6840–6855.
14. Liu, Y.-S.; Chen, Y.-R.; Chen, Y.-C. Thermoelectric Efficiency in Nanojunctions: A Comparison between Atomic Junctions and Molecular Junctions. *ACS Nano* **2009**, *3*, 3497–3504.
15. Cardamone, D. M.; Stafford, C. A.; Mazumdar, S. Controlling Quantum Transport through a Single Molecule. *Nano Lett.* **2006**, *6*, 2422.
16. Ke, S.-H.; Yang, W.; Baranger, H. U. Quantum Interference Controlled Molecular Electronics. *Nano Lett.* **2008**, *8*, 3257.
17. Tao, N. J. Electron Transport in Molecular Junctions. *Nat. Nanotechnol.* **2006**, *1*, 173–181.
18. Luttinger, J. M. Fermi Surface and Some Simple Equilibrium Properties of a System of Interacting Fermions. *Phys. Rev.* **1960**, *119*, 1153–1163.
19. Mayor, M.; Weber, H. B.; Reichert, J.; Elbing, M.; von Hänisch, C.; Beckmann, D.; Fischer, M. Electric Current through a Molecular Rod-Relevance of the Position of the Anchor Groups. *Angew. Chem., Int. Ed.* **2003**, *42*, 5834–5838.
20. Kassubek, F.; Stafford, C. A.; Grabert, H. Force, Charge, and Conductance of an Ideal Metallic Nanowire. *Phys. Rev. B* **1999**, *59*, 7560–7574.
21. Zangmeister, C. D.; Robey, S. W.; van Zee, R. D.; Yao, Y.; Tour, J. M. Fermi Level Alignment and Electronic Levels in Molecular Wire Self-Assembled Monolayers on Au. *J. Phys. Chem. B* **2004**, *108*, 16187–16193.
22. Stafford, C. A.; Kotlyar, R.; Das Sarma, S. Coherent Resonant Tunneling through an Artificial Molecule. *Phys. Rev. B* **1998**, *58*, 7091.
23. Castleton, C. W. M.; Barford, W. Screening and the Quantitative π-Model Description of the Optical Spectra and Polarizations of Phenyl Based Oligomers. *J. Chem. Phys.* **2002**, *117*, 3570–3582.